

20. Anton van der Merwe, P., Davis, S. J. & Dustin, M. L. Cytoskeletal polarization and redistribution of cell-surface molecules during T cell antigen recognition. *Semin. Immunol.* **12**, 5–21 (2000).
21. Cunningham, B. C. *et al.* Dimerization of the extracellular domain of the human growth hormone receptor by a single hormone molecule. *Science* **254**, 821–825 (1991).
22. Plotnikov, A. N., Schlessinger, J., Hubbard, S. R. & Mohammadi, M. Structural basis for FGF receptor dimerization and activation. *Cell* **98**, 641–650 (1999).
23. Wilson, I. A. & Jolliffe, L. K. The structure, organization, activation and plasticity of the erythropoietin receptor. *Curr. Opin. Struct. Biol.* **9**, 696–704 (1999).
24. Luo, R. Z., Beniac, D. R., Fernandes, A., Yip, C. C. & Ottensmeyer, F. P. Quaternary structure of the insulin–insulin receptor complex. *Science* **285**, 1077–1080 (1999).
25. Otwinowski, Z. & Minor, W. Processing of X-ray diffraction data collected in oscillation mode. *Methods Enzymol.* **176**, 307–326 (1997).
26. Brunger, A. T. *et al.* Crystallography & NMR system: a new software suite for macromolecular structure determination. *Acta. Crystallogr. D* **54**, 905–921 (1998).
27. Jones, T. A., Cowan, S., Zou, J. Y. & Kjeldgaard, M. Improved methods for building protein models in electron density maps and the location of errors in these models. *Acta Crystallogr. A* **47**, 110–119 (1991).
28. Laskowski, R. A., MacArthur, M. W. & Thornton, J. M. Validation of protein models derived from experiment. *Curr. Opin. Struct. Biol.* **8**, 631–639 (1998).
29. Lawrence, M. C. & Colman, P. M. Shape complementarity at protein/protein interfaces. *J. Mol. Biol.* **234**, 946–950 (1993).
30. Evans, S. V. SETOR: hardware-lighted three-dimensional solid model representations of macromolecules. *J. Mol. Graph.* **11**, 134–138 (1993).
31. Barton, G. J. Protein multiple sequence alignment and flexible pattern matching. *Methods Enzymol.* **183**, 403–428 (1990).
32. Holm, L. & Sander, C. Dali: a network tool for protein structure comparison. *Trends Biochem. Sci.* **20**, 478–480 (1995).

**Acknowledgements**

We thank M. Scharff, P. Scherer, A. Davidson, A. Bresnick, T. DiLorenzo, A. Kalergis and M. Roden for comments. We also thank K. Rajashankar for assistance with data collection. This work was supported by grants from the National Institute of Allergies and Infectious Diseases. We acknowledge the support of the Albert Einstein Comprehensive Cancer Center.

Correspondence and requests for materials should be addressed to S.C.A. (e-mail: almo@aecom.yu.edu) or S.G.N. (e-mail: nathenso@aecom.yu.edu).

**Crystal structure of the B7-1/CTLA-4 complex that inhibits human immune responses**

**Carin C. Stamper\*†, Yan Zhang\*†, James F. Tobin\*, David V. Erbe\*, Shinji Ikemizu‡, Simon J. Davis§, Mark L. Stahl\*, Jasbir Seehra\*, William S. Somers\* & Lidia Mosyak\***

\* Departments of Biological Chemistry and Musculoskeletal Sciences, Wyeth Research, 87 Cambridge Park Drive, Cambridge, Massachusetts 02140, USA

‡ Division of Structural Biology, The Henry Wellcome Building for Genomic Medicine, The University of Oxford, Roosevelt Drive, Oxford OX3 7BN, UK

§ Nuffield Department of Clinical Medicine, The University of Oxford, John Radcliffe Hospital, Headington, Oxford OX3 9DU, UK

Optimal immune responses require both an antigen-specific and a co-stimulatory signal. The shared ligands B7-1 and B7-2 on antigen-presenting cells deliver the co-stimulatory signal through CD28 and CTLA-4 on T cells. Signalling through CD28 augments the T-cell response, whereas CTLA-4 signalling attenuates it. Numerous animal studies<sup>1,2</sup> and recent clinical trials<sup>3,4</sup> indicate that manipulating these interactions holds considerable promise for immunotherapy. With the consequences of these signals well established, and details of the downstream signalling events emerging<sup>5–7</sup>, understanding the molecular nature of these extracellular interactions becomes crucial. Here we report the crystal structure of the human CTLA-4/B7-1 co-stimulatory complex at 3.0 Å resolution. In contrast to other interacting cell-surface

molecules, the relatively small CTLA-4/B7-1 binding interface exhibits an unusually high degree of shape complementarity. CTLA-4 forms homodimers through a newly defined interface of highly conserved residues. In the crystal lattice, CTLA-4 and B7-1 pack in a strikingly periodic arrangement in which bivalent CTLA-4 homodimers bridge bivalent B7-1 homodimers. This zipper-like oligomerization provides the structural basis for forming unusually stable signalling complexes at the T-cell surface, underscoring the importance of potent inhibitory signalling in human immune responses.

The extracellular domains of human soluble (s) CTLA-4, residues 3–125 (SWISSPROT numbering), and sB7-1, residues 1–214, were expressed in Chinese hamster ovary (CHO) cells. The complex containing fully glycosylated sCTLA-4 and sB7-1 was crystallized in the space group C222<sub>1</sub>. In the crystal lattice, sCTLA-4 and sB7-1 monomers each associate as non-crystallographic, roughly two-fold symmetric homodimers; single copies of each homodimer together form the asymmetric unit (Fig. 1a). The association of the four monomers in the asymmetric unit is driven by the interaction of three surfaces: the surface mediating sB7-1 homodimerization; the CTLA-4 homodimer interface; and the receptor–ligand binding interface.

The structures of the uncomplexed sCTLA-4 (refs 8, 9) and sB7-1

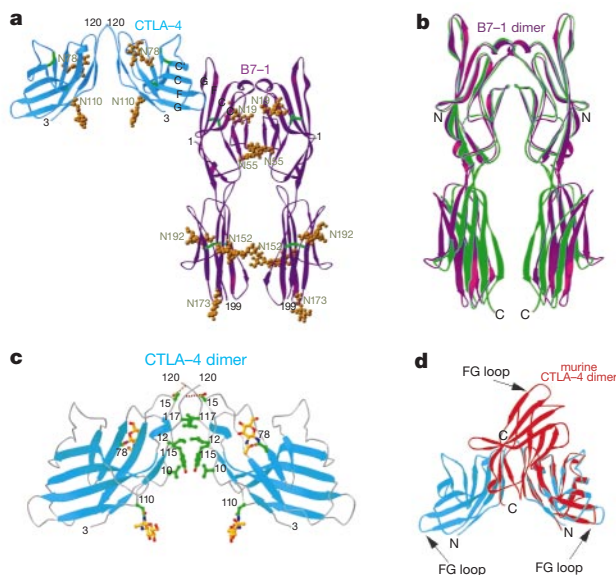


**Figure 1** Structural comparison of sCTLA-4/sB7-1 complex with uncomplexed forms of sCTLA-4 and sB7-1. **a**, Ribbon diagram of the sCTLA-4/sB7-1 complex showing two sB7-1 (purple) and two sCTLA-4 (cyan) molecules in the asymmetric unit. Disulphide bonds (green) and sugar moieties (yellow) are also shown.  $\beta$ -sheets involved in the receptor–ligand interaction are labelled. Glycosylation sites on sCTLA-4 (Asn 78 and Asn 110) and on sB7-1 (Asn 19, Asn 55, Asn 152, Asn 173 and Asn 192) are all surface exposed. None of the ordered glycosides is involved in the receptor–ligand recognition. **b**, Superposition of the ligand-binding V-set domains of complexed (purple ribbons) and uncomplexed (cyan ribbons) forms of sB7-1. Apparent displacement of the membrane-proximal domains does not affect the interactions at the interdomain regions and is perhaps a result of differences in crystal packing contacts. **c**, Detailed view of the sCTLA-4 homodimer interface. Residues involved in hydrophobic interactions between the two monomers are shown in green. Two hydrogen bonds formed at the elbow of the homodimer are indicated as red dashed lines. Spatial proximity of the C termini (Glu 120) would enable a formation of disulphide bond between cysteines at positions 122. Asn 110 is the only strictly conserved glycosylation site in CTLA-4 and CD28. Located between the two monomers, N-glycans in these positions might stabilize the homodimer. **d**, Superposition of human sCTLA-4 dimer (cyan) on murine sCTLA-4 dimer (red). From this orientation, the contradiction between the two dimerization modes is evident. R.m.s. deviation between the two individual monomers is 1.5 Å for 114 C $\alpha$  pairs. The FG loop of sCTLA-4 in the complex is displaced by 2.5 Å toward sB7-1. Figure prepared with RIBBONS<sup>29</sup>.

† Present address: Pfizer Cambridge Discovery Technology Center, 620 Memorial Drive, Cambridge, Massachusetts 02139, USA.

(ref. 10) have shown that the two proteins comprise, respectively, a single V-set, and paired V-set and C1-set immunoglobulin superfamily (IgSF) domains. Overall, the sCTLA-4 and sB7-1 monomers do not show any significant conformational rearrangements on complex formation, apart from small local changes restricted to their binding sites. The glycosylated sB7-1 homodimer seen in the crystals of the complex is essentially identical to that observed in crystals of deglycosylated sB7-1 (ref. 10): the monomer–monomer interface is the same size ( $570 \text{ \AA}^2$  per monomer; calculated using the program SURFACE<sup>11</sup>; probe radius  $1.4 \text{ \AA}$ ) and involves the same residues. When the V-set domains of the two sB7-1 homodimers are superimposed (Fig. 1b), the membrane-proximal C1-set domains are displaced by only  $3 \text{ \AA}$ . Similar variation has been observed in individual crystals of sB7-1 (S.I. *et al.*, unpublished data), suggesting that these differences are more likely to result from variability in sB7-1 self-association than from the effects of ligand binding. sB7-1 homodimerization has been confirmed in solution using analytical ultracentrifugation methods<sup>10</sup>.

Although the structure of the sCTLA-4 monomer is very similar to that of the murine sCTLA-4 monomer<sup>8</sup>, the human and murine<sup>8</sup> sCTLA-4 homodimers observed in the two lattices are very different (Fig. 1c, d). Of the two structures, we consider that the sCTLA-4 homodimer present in the crystals of the complex represents the more plausible model for native CTLA-4. First, all of the interacting residues are strictly conserved, in contrast to the conservation of only four of the ten residues forming the murine dimer interface<sup>8</sup>. Second, the human sCTLA-4 homodimer is not precluded by glycosylation. If used as in human CTLA-4 (ref. 12), an N-linked glycan at the conserved Asn 78 glycosylation site would prevent murine-like homodimerization in all species. Third, the human homodimer allows co-ligation of sB7-1 molecules around an axis orthogonal to the membrane, maintaining the  $\sim 140 \text{ \AA}$  intermembrane distance thought to be a critical feature of the immunological synapse<sup>5</sup>. Last, the interchain disulphide bond will more readily form in the human sCTLA-4 homodimer. The  $7.7 \text{ \AA}$  spacing between the C $\alpha$  atoms of the last visible residue in each monomer (Pro 119) is more likely to be bridged by the three additional residues and by the disulphide bond in the human sCTLA-4 dimer than is the equivalent  $30.1 \text{ \AA}$  distance in the murine structure. Consequently, the murine model for CTLA-4 dimerization and signalling proposed previously<sup>8</sup> is most probably not relevant to the formation of co-stimulatory complexes.

The human sCTLA-4 monomers interact through residues in the

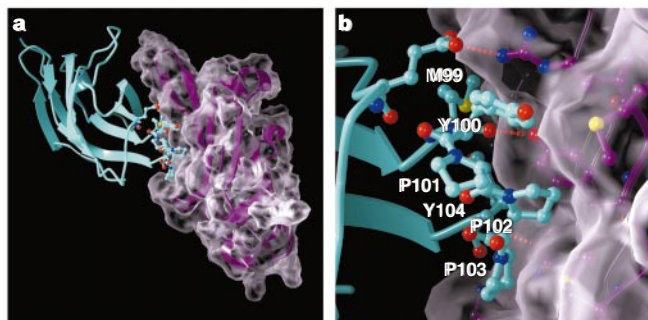


**Figure 2** Overview of receptor–ligand interactions. **a**, Ribbon diagram showing orthogonal interaction between sCTLA-4 (cyan) and sB7-1 (purple) monomers. Also shown is the molecular surface representation (white transparent) of the ligand-binding domain of sB7-1 to emphasize the high geometric match between the two interacting surfaces. **b**, Direct receptor–ligand contacts. The <sup>99</sup>MYPPPY<sup>104</sup> loop of sCTLA-4 is buried in a shallow depression of the sB7-1 GFCC' surface. Colour coding is as in **a**. Three out of five hydrogen bonds formed across the  $\beta$ -sheets of the interacting domains are depicted as red dashed lines. Several other side chains on CTLA-4 and B7-1 (not shown) may contribute to the binding through appreciable, but not direct, contacts formed on the periphery of the binding interface. Figure prepared with BobScript<sup>30</sup>.

A and G  $\beta$ -strands (Val 10, Leu 12, Ser 15, Tyr 115, Ile 117, Glu 120), burying only  $460 \text{ \AA}^2$  of surface<sup>11</sup> per monomer. The interface is essentially hydrophobic except for reciprocal, interchain hydrogen bonds between the side chain of Ser 15 and the main-chain nitrogen of Glu 120 at the elbow of the homodimer (Fig. 1c). This weak interaction might explain why, in the absence of the interchain disulphide (Cys–Cys 122), sCTLA-4 is monomeric in solution (ref. 9; and Y.Z. and M.S., unpublished data). The amino acids mediating CTLA-4 dimerization are not conserved in CD28; however, the equivalent residues exhibit the same overall hydrophobicity, implying that CD28 might form similar homodimers.

Differences noted<sup>8</sup> between the murine structure and the human sCTLA-4 structure determined by NMR methods<sup>9</sup> are also seen in the complex crystals. In particular, the V-set domain has C'DEBA:GFCC' rather than DEBA:GFCC'C' topology, and the three consecutive prolines in the FG loop, MY<sup>101</sup>PPP<sup>103</sup>Y, adopt the *cis*–*trans*–*cis* rather than *trans*–*trans*–*cis* conformation seen in the NMR structure<sup>9</sup>. This has important implications for B7-1 binding (see below).

Mutational data have implicated the membrane-proximal domain of B7-1 in interactions with CTLA-4 and CD28 (ref. 13), but these effects must have been indirect as sCTLA-4 only contacts residues of the sB7-1 V-set domain. Receptor–ligand binding occurs through the GFCC' face of the sCTLA-4 and sB7-1 V-set domains, with a roughly  $90^\circ$  angle between the interacting  $\beta$ -sheets (Fig. 2a). In this orientation, the FG, BC and C'C' loops of sCTLA-4 extend across the base of the sB7-1 five-stranded  $\beta$ -sheet, burying a total of  $1,255 \text{ \AA}^2$  of solvent-accessible surface<sup>11</sup> ( $600 \text{ \AA}^2$  from sB7-1 and  $655 \text{ \AA}^2$  from sCTLA-4). These values are at the low end of the range for protein–protein binding sites ( $600$ – $900 \text{ \AA}^2$ )<sup>14</sup>.

Orthogonal binding mediated by the GFCC'C' face of the V-set IgSF domains of cell-surface molecules was first seen in rat and human sCD2 crystal contacts<sup>15,16</sup>, and subsequently in the native complex of sCD2 and sLFA-3 (ref. 17) and in crystals of the coxsackie virus and adenovirus receptor<sup>18</sup>. It seems likely that this orthogonal binding mode will be a recurrent theme of V-set interactions. There is no compelling reason why such orthogonal interactions should have arisen through convergent evolution, but it is possible that these complexes bear the imprint of primordial IgSF interactions.

Interatomic contacts (85 total; van der Waals radius  $3.9 \text{ \AA}$ ) are made between 13 residues of CTLA-4 residues and 13 residues of

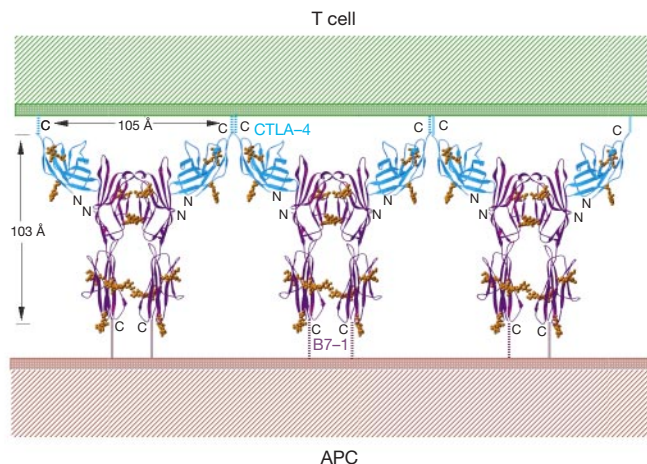


**Figure 3** Molecular association of sCTLA-4 and sB7-1 in the crystal lattice. Shown are 'skewed zipper' arrays in which sCTLA-4/sB7-1 complexes would be evenly spaced along membrane surfaces with a separation of  $105 \text{ \AA}$ . In the perpendicular direction, across membranes, ligated receptors would span  $140 \text{ \AA}$ . Geometrically, sugar chains attached at Asn 173 on B7-1 (bottom) are close to the cell membrane, implying their potential involvement in interaction with the membrane, perhaps by stabilizing the orientation of the B7-1 dimers. APC, antigen-presenting cell. Figure prepared with RIBBONS<sup>29</sup>.

B7-1. Most of these are hydrophobic contacts, but there are also five hydrogen bonds. The FG loop of sCTLA-4, which contains the hydrophobic <sup>99</sup>MYPPPY<sup>105</sup> sequence that is strictly conserved in CTLA-4 and CD28, dominates the interaction and contributes 400 Å<sup>2</sup> of protein surface<sup>11</sup> to the binding interface (Fig. 2b). The FG loop makes hydrophobic contacts with a largely nonpolar surface of sB7-1 consisting of Tyr 31, Met 38, Thr 41, Met 43, Val 83, Leu 85, Ala 91, Phe 92 and Leu 97.

Mutations of the two central residues, Tyr 31 and Met 38, disrupt B7-1 binding to CTLA-4 and CD28 (ref. 13); the other residues forming this surface have not been tested. Five hydrogen bonds, including one between the charged residues Glu 33 on sCTLA-4 and Arg 29 on sB7-1 are likely to contribute to the specificity of binding (Fig. 2b). All residues in the <sup>99</sup>MYPPPY<sup>105</sup> sequence, except Pro 101, are in direct contact with sB7-1, and all alanine substitutions of these residues, including Pro 101, reduce or abolish binding to B7-1 (ref. 9). Analysis of the complex structure indicates that the crucial role of Pro 101 is to initiate the *cis-trans-cis* main-chain conformation of the FG loop, directing Tyr 100, Pro 102, Pro 103 and Tyr 104 towards interactions with sB7-1. At the core of the interface, Pro 102 of CTLA-4 and Tyr 31 of B7-1 participate in a stacking interaction (Figs 2b, 4) that is likely to be conserved both across species and in interactions involving CD28 and B7-2 (in B7-2 Tyr 31 is replaced by phenylalanine).

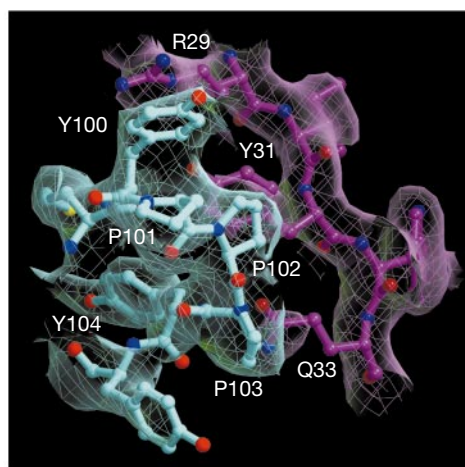


**Figure 4** A 3 Å resolution electron-density map in the region of the receptor–ligand binding site. Electron density is from an annealed omit map calculated using the  $3F_{\text{obs}} - 2F_{\text{calc}}$  amplitudes and model phases, with the CTLA-4 atoms excluded from the refinement and all calculations. The map is contoured at  $1\sigma$  level. Colour coding is as in Figs 1 and 2.

**Table 1** Statistics for data collection and refinement

Data collection		
Resolution range (Å)	20–3.0	3.11–3.0
Completeness (%)	99.2	94.1
Total observations	209,381	–
Unique reflections	38,815	3,636
Average $I/\sigma(I)$	19.1	3.0
$R_{\text{sym}}^*(\%)$	6.7	35.1
Model refinement		
Maximum resolution (Å)	3.0	
Number of reflections (free)	$F_{\text{obs}} > 2\sigma$ 31,410 (1,887)	$F_{\text{obs}} > 0\sigma$ 35,465
$R_{\text{work}}/R_{\text{free}}$ †(%)	23.1/25.9	25.3/28.2
r.m.s. deviations		
Bonds (Å)	0.010	
Angles (°)	1.48	

\*  $R_{\text{sym}} = \sum |I_h - \langle I_h \rangle| / \sum I_h$ , where  $\langle I_h \rangle$  is the average intensity over symmetry equivalents. Numbers in the second column reflect statistics for the last resolution shell.  
†  $R_{\text{work}} = \sum |F_{\text{obs}} - |F_{\text{calc}}|| / \sum |F_{\text{obs}}|$ .  $R_{\text{free}}$  is equivalent to  $R_{\text{work}}$ , but calculated for a randomly chosen 6% of reflections omitted from the refinement process.

Accordingly, the two binding surfaces exhibit a very high degree of shape complementarity. An algorithm<sup>19</sup> measuring the degree of geometric fit between two protein surfaces gives scores of 0.74–0.77 for the sCTLA-4/sB7-1 binding interface. This value is similar to those for constitutive oligomeric proteins (0.7–0.76) and much higher than scores for protein antigen–antibody interfaces (0.64–0.68) or interacting cell-surface molecules (0.45–0.58; ref. 17 and references therein). This degree of complementarity accounts for the enthalpy-driven nature of binding (R. O’Brien *et al.*, personal communication), whereas the small interacting surfaces and slightly unfavourable entropy explain the very fast binding kinetics<sup>12</sup>.

In the crystal lattice, the sCTLA-4 and sB7-1 homodimers pack together to form a periodic arrangement in which bivalent sCTLA-4 homodimers bridge bivalent sB7-1 homodimers (Fig. 3). The sB7-1 and shorter CTLA-4 homodimers associate orthogonally, thus generating a ‘skewed zipper’ arrangement. It has long been clear that CTLA-4 exists as a constitutive, bivalent homodimer, and the affinity of sB7-1 self-association (dissociation constant,  $K_d = 20\text{--}50 \mu\text{M}$ ) indicates that B7-1 is also likely to exist as a dimer at the cell surface, albeit in dynamic monomer–dimer equilibrium<sup>10</sup>. We therefore expect oligomeric arrays that are similar, if not identical, to those seen in the crystals to form at the membrane interface between T cells and antigen-presenting cells.

Including the ‘stalk’ regions, the extracellular domains of the ligated receptors are expected to span a distance of  $\sim 140 \text{Å}$  between the opposing cell membranes, a distance compatible with that required by T-cell receptor (TCR)–MHC, natural killer cell inhibitory receptor (KIR)–MHC or CD2–CD58 intercellular interactions<sup>5,17,20,21</sup>. Overall, this arrangement is reminiscent of the ‘cell-adhesion zipper’ observed in the crystals of cadherins, which is thought to be a fundamental feature in adhesive interactions between cells expressing these molecules<sup>22</sup>.

As far as is generally known, cell-surface molecules bind their ligands monovalently and with very low (micromolar) affinities<sup>23</sup>. The submicromolar affinity of B7-1 for CTLA-4 ( $K_d = 0.2\text{--}0.4 \mu\text{M}$ ; ref. 12) is thus unusually high for interacting cell-surface molecules. Our structural analysis of the complex implies that potent B7-mediated inhibitory signalling is not based exclusively on the stability of association between individual homodimers, but rather that the counter-receptor oligomeric arrays will also strengthen the interaction between the opposing cells. The combination of sub-micromolar affinity and oligomeric, high-avidity binding is, to our knowledge, unique to CTLA-4/B7-1 interactions.

The amplification and attenuation of TCR signalling occurs in a specialized contact area on the cell surface, termed the immunological synapse<sup>5,6</sup>, through the recruitment of receptors and their signalling complexes that effect the phosphorylation state of the TCR (ref. 7). Notably, inhibition of TCR signalling by CTLA-4 has been seen only to occur when both signals are delivered by the same cell surface<sup>24</sup>; however, other data suggest that the regulatory signals delivered by CD28 and CTLA-4 may not be strictly cell autonomous<sup>25</sup>. Regardless of the precise nature of the signals and mechanisms involved, it now seems that the inhibition of immune responses by CTLA-4 requires the formation of unusually stable complexes, the structure of which is revealed by the crystals of sCTLA-4/sB7-1. Whether such stable complexes are required for the efficient use of low-abundance CTLA-4 molecules at the T-cell surface, or enhance the potency of inhibitory CTLA-4 signalling by concentrating key effector molecules such as the phosphatase SHP-2 (ref. 7) under the immunological synapse, or both, remains to be established. □

## Methods

### Production and purification of B7-1 and CTLA-4

Constructs encoding the extracellular portions of human CTLA-4 or B7-1 were fused to an enterokinase cleavage sequence (DYKDDDDK) followed by the IgG1 CH2–CH3 domains, and expressed in CHO cells. In addition, the cysteine at position 122 of CTLA-4

was mutated to serine. These were recovered from conditioned medium by protein-A chromatography, cleaved with enterokinase, further purified and confirmed to be monomeric by gel-filtration chromatography as described<sup>26</sup>. Appropriate binding characteristics for each protein were confirmed by surface plasmon resonance (Biacore) analysis and found to be consistent with published values<sup>12</sup>. For CTLA-4, the final cleaved protein comprised residues 3–125 (with the C122S mutation) followed by the octa-peptide DYKDDDDK at the carboxy terminus. For B7-1, the cleaved protein consisted of residues 1–214 with the DYKDDDDK octa-peptide again forming the C terminus.

**Crystallization and data collection**

The B7-1/CTLA4 complex was formed by incubating a 1:1.5 molar ratio of B7-1 and CTLA4 and purified using a TSK-3000SW size exclusion column (TosoHaas). The purified complex was buffer exchanged and concentrated to 10 mg ml<sup>-1</sup> in 20 mM Tris-HCl, pH 8.0. Crystals were grown at 18 °C by the hanging drop method by combining 2 µl of protein solution with 2 µl of 14% PEG 8000, 200 mM magnesium acetate and 100 mM cacodylate, pH 6.3, and equilibrated against 1 ml of the same solution. Crystals appeared in 5 days and were soaked in 16% PEG 8000, 200 mM magnesium acetate, 20 mM Tris-HCl pH 8.0, 100 mM cacodylate, pH 6.3, 20% ethylene glycol for about 1 min before plunging into liquid nitrogen. Crystals belong to space group C222<sub>1</sub> with unit-cell dimensions *a* = 88.5, *b* = 183.4, *c* = 230.8 Å and a calculated solvent content of 58% for two B7-1 and two CTLA-4 molecules per asymmetric unit (adding 82,000 (82K) of glycosylation estimated from SDS-PAGE gel mobility). The 3.0 Å resolution data were collected from a single crystal at 100K at Beamline 5.0.2 at the Advanced Light Source using a Quantum 4 CCD. 725 0.2° rotation images were collected and reduced with HKL2000 (ref. 27) giving statistics outlined in Table 1.

**Structure determination and refinement**

The structure was solved by molecular replacement in CNS<sup>28</sup> using the crystallographic dimer observed in the human B7-1 structure as the search model<sup>10</sup>. After rigid body refinement of each B7-1 domain the *R* factor was 55.3%. Initial electron-density maps phased with B7-1 alone showed clear electron density for the two CTLA-4 molecules. The model of murine CTLA-4 monomer (PDB accession number 1dqt) was placed into electron density and was manually rebuilt in QUANTA (Molecular Simulations) to reflect the sequence of human CTLA-4. Non-conserved amino-acid residues and loop regions of CTLA-4 and B7-1, as well as sugar moieties, were entirely built into electron density. A composite annealed omit map was calculated to check the conformation of CTLA-4 and B7-1 loop regions. All refinement procedures were done in CNS and used data from 20.0–3.0 Å. A 2σ cut-off was applied during the refinement because of the anisotropy of the data. Six per cent of the reflections were randomly selected for generation of the *R*<sub>free</sub> data set (see Table 1). The anisotropy of the data was corrected for also using CNS.

Tight non-crystallographic symmetry restraints were gradually relaxed during the refinement process resulting in a final model with *R*<sub>work</sub> of 23.2% and *R*<sub>free</sub> of 25.9%. Continuous electron density was seen for sugar moieties at four N-linked carbohydrate sites on CTLA-4 dimer (Asn 78 and Asn 110) and at ten glycosylation sites on B7-1 dimer (Asn 19, Asn 55, Asn 152, Asn 173 and Asn 192). No saccharides could be modelled at six other expected glycosylation sites on B7-1 (Asn 64, Asn 177 and Asn 198). The final model contains two B7-1 molecules (residues A1–A199 and B1–B199), two CTLA-4 molecules (residues C3–C120 and D3–D120), 20 monosaccharides and shows reasonable geometry: 98.9% of non-glycine φ and ψ angles lie in the allowed regions of the Ramachandran plot (77.6% in the most favoured regions and 21.4% in additionally allowed regions); six amino-acid residues (1.1%) have disallowed angles.

Received 27 December 2000; accepted 9 February 2001.

1. Lenschow, D. J., Walunas, T. L. & Bluestone, J. A. CD28/B7 system of T cell costimulation. *Annu. Rev. Immunol.* **14**, 233–258 (1996).
2. Greenfield, E. A., Nguyen, K. A. & Kuchroo, V. K. CD28/B7 costimulation: a review. *Crit. Rev. Immunol.* **18**, 389–418 (1998).
3. Guinan, E. C. *et al.* Transplantation of anergic histoincompatible bone marrow allografts. *N. Engl. J. Med.* **340**, 1704–1714 (1999).
4. Abrams, J. R. *et al.* Blockade of T lymphocyte costimulation with cytotoxic T lymphocyte-associated antigen 4-immunoglobulin (CTLA4Ig) reverses the cellular pathology of psoriatic plaques, including the activation of keratinocytes, dendritic cells, and endothelial cells. *J. Exp. Med.* **192**, 681–694 (2000).
5. van der Merwe, P. A., Davis, S. J., Shaw, A. S. & Dustin, M. L. Cytoskeletal polarization and redistribution of cell-surface molecules during T cell antigen recognition. *Semin. Immunol.* **12**, 5–21 (2000).
6. Grakoui, A. *et al.* The immunological synapse: a molecular machine controlling T cell activation. *Science* **285**, 221–227 (1999).
7. Lee, K.-M. *et al.* Molecular basis of T cell inactivation by CTLA-4. *Science* **282**, 2263–2266 (1998).
8. Ostrov, D. A., Shi, W., Schwartz, J.-C. D., Almo, S. C. & Nathenson, S. G. Structure of murine CTLA4 and its role in modulating T cell responsiveness. *Science* **290**, 816–819 (2000).
9. Metzler, W. J. *et al.* Solution structure of human CTLA4 and delineation of a CD80/CD86 binding site conserved in CD28. *Nature Struct. Biol.* **4**, 527–531 (1997).
10. Ikemizu, S. *et al.* Structure and dimerization of a soluble form of B7-1. *Immunity* **12**, 51–60 (2000).
11. Collaborative computational project No. 4. The CCP4 suite: Programs for protein crystallography. *Acta Crystallogr. D* **50**, 760–776 (1994).
12. van der Merwe, P. A., Bodian, D. L., Daenke, S., Linsley, P. & Davis, S. J. CD80 (B7-1) binds both CD28 and CTLA-4 with a low affinity and very fast kinetics. *J. Exp. Med.* **185**, 393–403 (1997).
13. Peach, R. J. *et al.* Both extracellular immunoglobulin-like domains of CD80 contain residues critical for binding T cell surface receptors CTLA-4 and CD28. *J. Biol. Chem.* **268**, 21181–21187 (1993).
14. Janin, J. & Chothia, C. The structure of protein-protein recognition sites. *J. Biol. Chem.* **265**, 16027–16030 (1990).
15. Jones, E. Y., Davis, S. J., Williams, A. F., Harlos, K. & Stuart, D. I. Crystal structure at 2.8 Å resolution of a soluble form of the cell adhesion molecule CD2. *Nature* **360**, 232–239 (1992).
16. Bodian, D. L., Jones, E. Y., Harlos, K., Stuart, D. I. & Davis, S. J. Crystal structure of the extracellular

- region of the human cell adhesion molecule CD2 at 2.5 Å resolution. *Structure* **15**, 755–766 (1994).
17. Wang, J.-h. *et al.* Structure of a heterophilic adhesion complex between the human CD2 and CD58 (LFA-3) counterreceptors. *Cell* **7**, 791–803 (1999).
18. van Raaij, M. J., Chouin, E., van der Zandt, H., Bergelson, J. M. & Cusack, S. Dimeric structure of the coxsackievirus and adenovirus receptor D1 domain at 1.7 Å resolution. *Struct. Fold Des.* **8**, 1147–1155 (2000).
19. Lawrence, M. C. & Colman, P. M. Shape complementarity at protein/protein interfaces. *J. Mol. Biol.* **234**, 946–950 (1993).
20. Garboczi, D. N. *et al.* Structure of the complex between human T-cell receptor, viral peptide and HLA-A2. *Nature* **384**, 134–141 (1996).
21. Boyington, J. C., Motyka, S. A., Schuck, P., Brooks A. G. & Sun, P. D. Crystal structure of an NK cell immunoglobulin-like receptor in complex with its class I MHC ligand. *Nature* **405**, 537–543 (2000).
22. Shapiro, L. *et al.* Structural basis of cell–cell adhesion by cadherins. *Nature* **374**, 327–337 (1995).
23. Davis, S. J., Ikemizu, S., Wild, M. K. & van der Merwe, P. A. CD2 and the nature of protein interactions mediating cell-cell recognition. *Immunol. Rev.* **163**, 217–236 (1998).
24. Griffin, M. D. *et al.* Blockade of T cell activation using a surface-linked single-chain antibody to CTLA-4 (CD152). *J. Immunol.* **164**, 4433–4442 (2000).
25. Bachmann, M. F., Kohler, G., Ecabert, B., Mak, T. W. & Kopf, M. Lymphoproliferative disease in the absence of CTLA-4 is not T cell autonomous. *J. Immunol.* **163**, 1128–1131 (1999).
26. Somers, W. S., Tang, J., Shaw, G. D. & Camphausen, R. T. Insights into the molecular basis of leukocyte tethering and rolling revealed by structures of P- and E-selectin bound to sLex and PSGL-1. *Cell* **103**, 467–479 (2000).
27. Otwinowski, Z. & Minor, W. Processing of X-ray diffraction data collected in oscillation mode. *Methods Enzymol.* **276**, 307–326 (1997).
28. Brunger, A. T. *et al.* Crystallography and NMR system (CNS): a new software suite for macromolecular structure determination. *Acta Crystallogr. D* **54**, 905–921 (1998).
29. Carson, M. Ribbons 2.0. *J. Appl. Crystallogr.* **24**, 958–961 (1991).
30. Esnouf, R. M. An extensively modified version of Molscrip that includes enhanced colouring capabilities. *J. Mol. Graph.* **15**, 132–134 (1997).

**Acknowledgements**

We thank R. Zollner and his colleagues for large scale cell culture, and D. I. Stuart and E. Y. Jones for helpful comments. We also thank the staff at Advanced Light Source for assistance with data collection. S.I. and S.J.D. are supported by the Wellcome Trust and the Human Frontier Science Programme.

Correspondence and requests for materials should be addressed to W.S.S. (e-mail: wsomers@genetics.com) or L.M (e-mail: lmosyak@genetics.com). The coordinates have been deposited in the Protein Data Bank. The accession code is 1I84.

.....  
**corrections**

**Genetic control and evolution of sexually dimorphic characters**

**Artyom Kopp, Ian Duncan, Dorothea Godt & Sean B. Carroll**

*Nature* **408**, 553–559 (2000).

The name of one author, Dorothea Godt, was omitted from the author list but is included above. She is affiliated with the Department of Zoology, University of Toronto, Canada. In addition, a gene name was misspelled: the correct spelling is bric à brac. □

**Mitochondrial genome variation and the origin of modern humans**

**Max Ingman, Henrik Kaessmann, Svante Pääbo & Ulf Gyllensten**

*Nature* **408**, 708–712 (2000).

The complete mtDNA sequences upon which the analyses are based can be found at our website (<http://www.genpat.uu.se/mtDB/>), dedicated to the analysis of complete mtDNA genomes of humans. The 53 sequences are also available in Genbank with the accession numbers AF346963–AF347015. □